


Cite this: *Nanoscale*, 2023, **15**, 14249

# High-efficiency all fluorescence white OLEDs with high color rendering index by manipulating excitons in co-host recombination layers†

Yuan-Bo Zhang,<sup>a</sup> Ya-Nan Li,<sup>a</sup> Chun-Fang Zhang,<sup>a</sup> Jia-Bo Liu,<sup>a</sup> Jia-Rui Li,<sup>a</sup> Hao-Dong Bian,<sup>a</sup> Lian-Qing Zhu,<sup>a</sup> Jian-Zhen Ou,<sup>b</sup> Lin-Song Cui<sup>\*c,d</sup> and Yuan Liu  <sup>\*a</sup>

All fluorescence white organic light-emitting diodes (WOLEDs) based on thermally activated delayed fluorescence (TADF) emitters are an attractive route to realize highly efficient and high color quality white light sources. However, harvesting triplet excitons in these devices remains a formidable challenge, particularly for WOLEDs involving conventional fluorescent emitters. Herein, we report a universal design strategy based on a co-host system and a cascaded exciton transfer configuration. The co-host system furnishes a broad and charge-balanced exciton generation zone, which simultaneously endows the devices with low efficiency roll-off and good color stability. A yellow TADF layer is put forward as an intermediate sensitizer layer between the blue TADF light-emitting layer (EML) and the red fluorescence EML, which not only constructs an efficient cascaded Förster energy transfer route but also blocks the triplet exciton loss channel through Dexter energy transfer. With the proposed design strategy, three-color all fluorescence WOLEDs reach a maximum external quantum efficiency (EQE) of 22.4% with a remarkable color rendering index (CRI) of 92 and CIE coordinates of (0.37, 0.40). Detailed optical simulation confirms the high exciton utilization efficiency. Finally, by introducing an efficient blue emitter 5Cz-TRZ, a maximum EQE of 30.1% is achieved with CIE coordinates of (0.42, 0.42) and a CRI of 84 at 1000 cd m<sup>-2</sup>. These outstanding results demonstrate the great potential of all fluorescence WOLEDs in solid-state lighting and display panels.

Received 31st May 2023,  
Accepted 3rd August 2023  
DOI: 10.1039/d3nr02568c

rs.c.li/nanoscale

## 1 Introduction

White organic light-emitting diodes (WOLEDs) nowadays have attracted great interest for flexible flat-panel displays and large-area solid-state lighting sources due to their merits of ultrathin form factor, low cost, high stretchability, and large-scale production.<sup>1–4</sup> OLEDs' electroluminescence (EL) performance is closely related to the exciton utilization in light-emitting layers (EMLs). To break through the 25% limit of exciton utilization in conventional fluorescent emitters, Baldo *et al.* developed phosphorescent emitters incorporating heavy metal

atoms to induce strong spin-orbit coupling, allowing 100% excitons to accomplish the radiation process.<sup>5</sup> However, the toxicity and rarity of heavy metals, increasing manufacturing costs, and lack of stable blue phosphorescence materials hinder the commercial application of all phosphorescence-based WOLEDs.<sup>6</sup> In 2012, Adachi *et al.* introduced purely organic thermally activated delayed fluorescence (TADF) materials that are generally composed of highly twisted electron donor-acceptor structures, featuring a small singlet-triplet energy gap ( $\Delta E_{ST}$ ).<sup>7</sup> In theory, TADF materials can achieve 100% internal quantum efficiency (IQE) because the generated triplet excitons can be harvested through the efficient reverse intersystem crossing (RISC) process induced by a sufficiently small  $\Delta E_{ST}$ . Moreover, TADF materials have donor and acceptor parts in one molecule, thus possessing natural bipolar properties, which are beneficial for charge balance in devices.<sup>8,9</sup> Currently, all three primary colors, *i.e.*, blue, green, and red TADF OLEDs, have realized comparable device performance to phosphorescent OLEDs, making TADF materials promising for commercialization.<sup>10–12</sup>

To make WOLEDs efficient light sources, three key kernels need to be satisfied: high external quantum efficiency (EQE),

<sup>a</sup>Key Laboratory of the Ministry of Education for Optoelectronic Measurement Technology and Instrument, Beijing Information Science & Technology University, No. 12 xiaoying East Road, Beijing, 100192, China. E-mail: yuan.liu@bistu.edu.cn

<sup>b</sup>School of Engineering, RMIT University, Melbourne, VIC 3000, Australia

<sup>c</sup>Key Laboratory of Precision and Intelligent Chemistry, University of Science and Technology of China, Hefei, Anhui, 230026, China. E-mail: lscui@ustc.edu.cn

<sup>d</sup>CAS Key Laboratory of Soft Matter Chemistry, Department of Polymer Science and Engineering, University of Science and Technology of China, Hefei, Anhui, 230026, China

† Electronic supplementary information (ESI) available. See DOI: <https://doi.org/10.1039/d3nr02568c>

high power efficiency, and low efficiency roll-off.<sup>2,13–15</sup> To reach high EQE, plenty of TADF materials with ~100% photoluminescence quantum yield (PLQY) have been designed and synthesized.<sup>16</sup> More importantly, TADF materials can be utilized as triplet sensitizers for conventional fluorescent (CF) emitters, named “hyperfluorescence”.<sup>17,18</sup> The hyperfluorescence system makes harvesting triplet excitons possible for fluorescent emitters and achieves an EQE of more than 15%. In particular, due to the diversity and low cost of CF emitters, it is undeniable that deep blue or red CF emitters are usually one of the necessary materials for preparing WOLEDs with high color rendering index (CRI).<sup>19,20</sup> In terms of power efficiency, the lower driving voltage is critical. For TADF materials, a host–guest system is usually adopted to dilute the concentration of emitters and improves the charge recombination efficiency. To confine the excitons, hosts need to satisfy high triplet energy to suppress guest-to-host energy back transfer. Considering the natural singlet–triplet energy offset and exciton binding energy, the host–guest system usually results in high driving voltages. Moreover, TADF emitters are sensitive to the polarity of the host materials, making the selection of hosts challenging.<sup>21–23</sup> Lots of strategies using materials such as bipolar host materials, exciplex host materials, and TADF host materials are proposed to reduce the driving voltages and extend recombination zones.<sup>21,24</sup> Recently, taking advantage of the bipolar characteristics of TADF materials, some TADF devices with neat TADF emitting layers have been reported to reduce driving voltages. However, these molecules need to conquer the challenge of aggregate quenching and the available emitters are rare.<sup>6,25,26</sup> Considering the efficiency roll-off, the intrinsic endothermic RISC in TADF materials makes it challenging to reach a competitive RISC rate compared to the ISC rate.<sup>27</sup> This means the triplet excitons still dominate in the singlet–triplet equilibrium and lead to severe triplet–triplet annihilation (TTA) and singlet–triplet annihilation (STA), resulting in high efficiency roll-off in TADF devices. Increasing the triplet-to-singlet spin–flip rate through molecular design and diluting the exciton density by extending the recombination zone are two representative strategies to reduce the device efficiency roll-off.<sup>28</sup>

Herein, by introducing a co-host system in the EMLs, we prepared an efficient TADF yellow OLED with a maximum EQE of 31.7% as well as low efficiency roll-off. All fluorescence TADF-based two-color WOLEDs show maximum efficiencies of 26.1%, 71.3 cd A<sup>-1</sup>, and 76.8 lm W<sup>-1</sup>, with low efficiency roll-off and great color stability. We confirmed that the excellent performance of the two-color WOLEDs originates from the broadened and stable exciton recombination zone induced by co-hosts. Moreover, we adopted a conventional deep red fluorescent emitter DBP to improve the color quality of WOLEDs. By using a cascaded exciton transfer layer to construct efficient Förster energy transfer processes, all fluorescence three-color WOLEDs realized a maximum EQE of 22.4% and a CRI of 92. Finally, we implemented our design strategy in WOLEDs with the highly efficient blue emitters PPCzTrz and 5Cz-TRZ, reaching a maximum EQE of 29.5% and 30.1%, respectively.

## 2 Experimental section

### 2.1 General information

All the materials adopted were commercially purchased without further purification. 1,4,5,8,9,11-Hexaazatriphenylenehexacarbonitrile (HAT-CN), 1,1-bis[(di-4-tolylamino)phenyl]cyclohexane (TAPC), 4,4',4-tris(carbazol-9-yl)triphenylamine (TCTA), 4,4'-bis(carbazol-9-yl)biphenyl (CBP), 3,3'-di(9H-carbazol-9-yl)-1,1'-biphenyl (mCBP), 4,6-bis(3,5-di(pyridin-3-yl)phenyl)-2-methylpyrimidine, 4,6-bis(3,5-di-3-pyridinylphenyl)-2-methylpyrimidine (B3PYMPM), 8-hydroxyquinolinolitolithium (Liq), bis[2-(diphenylphosphino)phenyl]ether oxide (DPEPO), and 10,10'-(4,4'-sulfonylbis(4,1-phenylene))bis(9,9-dimethyl-9,10-dihydroacridine) (DMAC-DPS) were purchased from Xi'an Polymer Light Technology Corp. 2,8-Bis(diphenylphosphoryl)-dibenzo[*b,d*]furan (PPF) and 2,2'-(1,3-phenylene) bis[9-phenyl-1,10-phenanthroline] (PBPPhen) were purchased from PURI Materials Company. 5,10-Bis(4-(3,6-di-*tert*-butyl-9H-carbazol-9-yl)-2,6-dimethylphenyl)-5,10-dihydroboranthrene (*t*BuCzDBA), 5,10,15,20-tetraphenylbisbenz[5,6]indeno[1,2,3-*cd*:1',2',3'-*lm*]perylene (DBP), and 9-(5'-(4,6-diphenyl-1,3,5-triazin-2-yl)-[1,1':3',1''-terphenyl]-2-yl)-3,6-diphenyl-9H-carbazole (PPCzTrz) were purchased from Luminescence Technology Corp. (9,9',9'',9''',9''''-(6-(4,6-Diphenyl-1,3,5-triazine-2-yl)benzene-1,2,3,4,5-pentayl) pentakis(9H-carbazole)) (5Cz-TRZ) was synthesized using reported methods.<sup>27</sup>

### 2.2 Fabrication and characterization of OLEDs

All OLEDs were fabricated according to the following steps. The patterned indium-tin-oxide (ITO, 110 nm)-coated glasses were used as substrates for OLEDs and subjected to a routine ultrasonic cleaning with a standard regiment of acetone, isopropanol, and deionized water for 5 min each. After that, all substrates were dried in an oven maintained at 120 °C. Before being transferred to the ultrahigh vacuum chamber, substrates were treated with oxygen plasma for 15 min. All materials were evaporated in a vacuum chamber (MBRAUN Co.) with a base pressure of 10<sup>-7</sup> mbar. The thickness and doping concentration of individual layers were *in situ* monitored by calibrated oscillating quartz-crystal sensors. After being encapsulated in a glove box, the current density–voltage–luminance (*J*–*V*–*L*) characteristics of the devices were measured using a system consisting of a Keithley 2420 SourceMeter, a silicon photodiode, and a calibrated spectrometer (Ocean Insight QE-PRO spectrometer). The EQE was measured in a calibrated integrating sphere (Ocean Insight SPECTRUMTEQ-EQY). The transient photoluminescence (PL) was achieved using a Hitachi fluorescence spectrometer F-4600.

## 3 Results and discussion

### 3.1 Co-host for monochrome TADF yellow OLEDs

High efficiency monochrome OLEDs are a prerequisite for realizing high efficiency all fluorescence WOLEDs. Here, we adopted an efficient yellow TADF dopant 9,10-bis(4-(3,6-di-*tert*-butyl-9H-carbazol-9-yl)-2,6-dimethylphenyl)-9,10-diboraan-

thracene (*t*BuCzDBA) that has a PLQY of 86% and a small  $\Delta E_{ST}$  of 22 meV.<sup>29</sup> The yellow OLED devices were fabricated with a structure of ITO/HAT-CN (5 nm)/TAPC (40 nm)/TCTA (10 nm)/host: 10% *t*BuCzDBA (20 nm)/PPF (10 nm)/PBPPPhen (50 nm)/LiQ (2 nm)/Al (100 nm). HAT-CN and LiQ were used as hole and electron injection layers, respectively. TAPC and PBPPPhen acted as hole and electron transport layers, respectively. TCTA and PPF with high triplet energies served as exciton-blocking layers to confine excitons in EMLs. CBP, PPF, CBP: PPF (1:1), mCBP: PPF (1:1), and TCTA: PPF (1:1) were employed as host materials for device Y1, device Y2, device Y3, device Y4, and device Y5, respectively.

Fig. 1a shows the current density–voltage–luminance ( $J$ – $V$ – $L$ ) characteristics of Y1–Y5. The co-host system (Y3, CBP: PPF) realizes lower driving voltage (shown in Table 1) compared with single-host devices Y1 (CBP) and Y2 (PPF). This can be attributed to the enhanced electron injection and transport capabilities in EMLs by introducing PPF, as shown in Fig. S1 (ESI<sup>†</sup>). To verify this hypothesis, we also compared mCBP: PPF (Y4) and TCTA: PPF (Y5) with their single-host counterparts, namely mCBP (Y6) and TCTA (Y7), respectively. All co-host devices exhibit lower driving voltages compared to single-host devices (Fig. S2 and S3, ESI<sup>†</sup>). This is consistent with previous reports.<sup>30</sup>

Single-host CBP based devices realized a maximum EQE of 26.9%. However, at low luminance, CBP undergoes an efficiency “roll-on” process which may be induced by its unbalanced charge that probably causes the large electron injection barrier from PPF to CBP (shown in Fig. S1, ESI<sup>†</sup>). CBP has proved to have bipolar charge-transport properties. However, the hole-transporting capability of CBP is much better than its electron-transporting capability due to the carbazole chemical unit.<sup>31</sup> At high luminance, the larger difference of hole and electron transport capability results in a narrow recombination zone and subsequent high efficiency roll-off. On the other hand, PPF is another excellent electron-type host material for TADF materials due to its high triplet energy (3.1 eV) and electron transport ability.<sup>32–34</sup> The single-host PPF based device achieves a maximum EQE of 28.5% but exhibits higher efficiency roll-off compared to single host CBP due to its unipolar properties. Compared with Y1 and Y2, the device Y3 with the CBP: PPF co-host exhibits a higher efficiency, indicating that a more balanced charge may be achieved. Maximum values of 31.7%, 93.3 cd A<sup>-1</sup>, and 104.6 lm W<sup>-1</sup> for EQE, current efficiency (CE), and power efficiency (PE), respectively, are achieved (Fig. 1b and Table 1). Noticeably, device Y3 also shows low efficiency roll-off at high luminance due to its broad recombination zone. The EQEs of Y3 at 100 cd m<sup>-2</sup> and 1000 cd m<sup>-2</sup> remain as high as 29.2% and 25.2%, respectively, corresponding to an efficiency roll-off of 7.9% and 20.5%. Device Y3 shows a spectrum peak at 567 nm, which is red-shifted by 10 nm compared to the EL spectrum of device Y1. This can be attributed to the different polarities of the host materials.<sup>29</sup> Like Y3, devices Y4 with mCBP: PPF co-host reaches a maximum EQE of 30.2% and exhibits similar efficiency roll-off. Meanwhile Y4 requires a higher driving voltage because mCBP has lower mobility compared to CBP due to its shorter conjugated length.<sup>35</sup> However, the TCTA: PPF co-host system only reaches a maximum EQE of 16.5%, though all TCTA, PPF, and TCTA: PPF exciplexes (Fig. S4, ESI<sup>†</sup>) have a higher triplet energy than *t*BuCzDBA, as shown in Fig. 1b. Excitons may be quenched by the host-emitter interactions in this device.<sup>22</sup> In addition, we explored the CBP: B3PYMPM co-host system, a well-known highly efficient exciplex system for green TADF materials (Fig. S4, ESI<sup>†</sup>).<sup>36,37</sup> Unfortunately, the maximum EQE of device Y8 is only 20.1%, which is significantly lower than that of device Y3 (Fig. S5, ESI<sup>†</sup>). All these results illustrate that excitons are efficiently utilized in the CBP: PPF co-host system and the CBP: PPF-based device exhibits better performance than a single-host device.

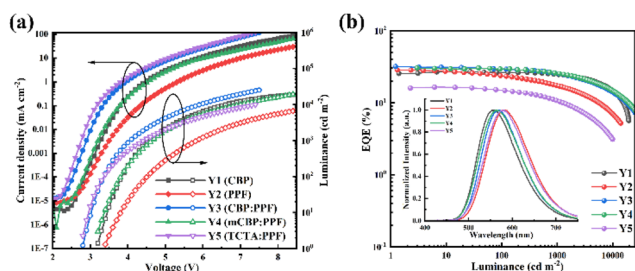


**Fig. 1** (a) Current density–voltage–luminance characteristics of devices Y1–Y5. (b) EQE–luminance curves of devices Y1–Y5. Insets in panel (b): the normalized EL spectra of Y1–Y5 at 10 mA cm<sup>-2</sup>.

**Table 1** Performance of monochrome yellow devices

Device	$V_{on}$ <sup>a</sup> (V)	$\eta_{EQE}$ <sup>b</sup> [%]	$\eta_{CE}$ <sup>b</sup> [cd A <sup>-1</sup> ]	$\eta_{PE}$ <sup>b</sup> [lm W <sup>-1</sup> ]	CIE <sup>c</sup>
Y1	3.2	26.9/26.4/24.5	83.0/81.5/75.6	77.0/67.4/51.6	(0.44, 0.54)
Y2	3.4	28.5/23.7/17.6	69.0/57.5/42.6	63.8/40.1/23.1	(0.50, 0.49)
Y3	2.8	31.7/29.2/25.2	93.3/85.8/73.9	104.6/82.6/59.5	(0.46, 0.52)
Y4	3.1	30.2/29.3/25.2	89.5/86.7/74.6	87.8/71.7/49.8	(0.45, 0.52)
Y5	2.7	16.5/15.3/10.8	43.3/40.0/28.3	47.3/38.1/20.2	(0.49, 0.50)
Y6	3.8	26.9/26.5/21.8	80.9/79.6/66.3	62.9/56.8/40.1	(0.44, 0.53)
Y7	3.0	12.7/10.5/7.9	34.3/28.6/21.8	35.9/23.6/13.7	(0.47, 0.51)
Y8	3.0	20.1/16.1/12.1	57.5/45.9/34.6	60.2/39.0/24.2	(0.43, 0.52)

<sup>a</sup> At a luminance of 1 cd m<sup>-2</sup>. <sup>b</sup> Efficiencies of the maximum, at 100 cd m<sup>-2</sup> and at 1000 cd m<sup>-2</sup>. <sup>c</sup> At a luminance of 1000 cd m<sup>-2</sup>.

lanced charge that probably causes the large electron injection barrier from PPF to CBP (shown in Fig. S1, ESI<sup>†</sup>). CBP has proved to have bipolar charge-transport properties. However, the hole-transporting capability of CBP is much better than its electron-transporting capability due to the carbazole chemical unit.<sup>31</sup> At high luminance, the larger difference of hole and electron transport capability results in a narrow recombination zone and subsequent high efficiency roll-off. On the other hand, PPF is another excellent electron-type host material for TADF materials due to its high triplet energy (3.1 eV) and electron transport ability.<sup>32–34</sup> The single-host PPF based device achieves a maximum EQE of 28.5% but exhibits higher efficiency roll-off compared to single host CBP due to its unipolar properties. Compared with Y1 and Y2, the device Y3 with the CBP: PPF co-host exhibits a higher efficiency, indicating that a more balanced charge may be achieved. Maximum values of 31.7%, 93.3 cd A<sup>-1</sup>, and 104.6 lm W<sup>-1</sup> for EQE, current efficiency (CE), and power efficiency (PE), respectively, are achieved (Fig. 1b and Table 1). Noticeably, device Y3 also shows low efficiency roll-off at high luminance due to its broad recombination zone. The EQEs of Y3 at 100 cd m<sup>-2</sup> and 1000 cd m<sup>-2</sup> remain as high as 29.2% and 25.2%, respectively, corresponding to an efficiency roll-off of 7.9% and 20.5%. Device Y3 shows a spectrum peak at 567 nm, which is red-shifted by 10 nm compared to the EL spectrum of device Y1. This can be attributed to the different polarities of the host materials.<sup>29</sup> Like Y3, devices Y4 with mCBP: PPF co-host reaches a maximum EQE of 30.2% and exhibits similar efficiency roll-off. Meanwhile Y4 requires a higher driving voltage because mCBP has lower mobility compared to CBP due to its shorter conjugated length.<sup>35</sup> However, the TCTA: PPF co-host system only reaches a maximum EQE of 16.5%, though all TCTA, PPF, and TCTA: PPF exciplexes (Fig. S4, ESI<sup>†</sup>) have a higher triplet energy than *t*BuCzDBA, as shown in Fig. 1b. Excitons may be quenched by the host-emitter interactions in this device.<sup>22</sup> In addition, we explored the CBP: B3PYMPM co-host system, a well-known highly efficient exciplex system for green TADF materials (Fig. S4, ESI<sup>†</sup>).<sup>36,37</sup> Unfortunately, the maximum EQE of device Y8 is only 20.1%, which is significantly lower than that of device Y3 (Fig. S5, ESI<sup>†</sup>). All these results illustrate that excitons are efficiently utilized in the CBP: PPF co-host system and the CBP: PPF-based device exhibits better performance than a single-host device.

### 3.2 Co-host for all fluorescence two-color WOLEDs

Inspired by the high EQE and low efficiency roll-off of device Y3, we further explored all fluorescence WOLEDs. DMAC-DPS was selected as the blue TADF. The complementary WOLED architecture was designed as ITO/HAT-CN (5 nm)/TAPC (40 nm)/TCTA (10 nm)/EML/PPF (10 nm)/PBPPPhen (50 nm)/LiQ (2 nm)/Al (100 nm). In device W1, CBP: PPF: *t*BuCzDBA (1:1, 10%, 7 nm)/mCBP: PPF: DMAC-DPS (1:1, 20%, 8 nm) was adopted as the white EML. In device W2, CBP: PPF: *t*BuCzDBA (1:1, 10%, 7 nm)/CBP: PPF: DMAC-DPS (1:1, 20%, 8 nm) was used as the white EML. We also prepared a single host EML

with a configuration of DPEPO:DMAC-DPS:*t*BuCzDBA (20%:1%, 15 nm) as the reference.

Fig. 2a shows the  $J$ - $V$ - $L$  curves for W1, W2, and W3. The co-host devices W1 and W2 show much lower driving voltages compared to that of single host W3, which can be attributed to the reduced recombination energy in the co-host system. Device W1 achieves a maximum EQE of 26.1%, which is comparable to the 25.5% maximum EQE of device W3. As DPEPO is a well-known efficient host material for DMAC-DPS, it is suggested that the excitons are completely harvested in W1. Notably, device W1 displays less efficiency roll-off compared to W3. For instance, it remains at 25.6% and 22.1% at the luminances of 100 and 1000  $\text{cd m}^{-2}$ , according to an efficiency roll-off of 1.9% and 15.3%, respectively (shown in Table 2). Benefiting from the low driving voltage and efficient exciton utilization, device W1 reaches a maximum luminance efficacy of 76.8  $\text{lm W}^{-1}$ . For W2, due to the lower triplet energy of CBP, energy transfer naturally occurs from DMAC-DPS to CBP, resulting in a serious exciton non-radiation process. As shown

in Fig. 2b, the EQE of device W2 is as low as 9.5%. Intriguingly, as shown in Fig. 2c, W1 shows great color stability in the luminance range of 1000–5000  $\text{cd m}^{-2}$ . We speculate that a great charge balance and a broad recombination zone are achieved in the co-host system. Meanwhile, W3 shows strong yellow emission in EL spectra, indicating efficient energy transfer from DMAC-DPS to *t*BuCzDBA (Fig. S6, ESI†). However, W3 shows reduced color stability compared to W1, which may be attributed to the saturation of the yellow emitter at high luminance.

To further validate the functionality of the co-host system, we also fabricated device W4 with a single-host emitting layer of CBP:*t*BuCzDBA (10%, 7 nm)/PPF:DMAC-DPS (20%, 8 nm) (device W4). As shown in Fig. S7,† device W4 shows a similar emission spectrum as device W1, with a CIE coordinate of (0.32, 0.42). Compared to W1, W4 shows higher efficiency roll-off and lower color stability, which can account for its narrow recombination zone, as shown in Fig. S8.†

To investigate the origin of high color stability and low efficiency roll-off of WOLEDs, hole- and electron-only devices were prepared to illustrate the bipolar characteristics of co-hosts. As shown in Fig. S9 (ESI†), both CBP:PPF and mCBP:PPF co-host systems exhibit excellent balanced carrier transport ability, as evidenced by their comparable current density at certain voltages. This effectively broadens the exciton recombination region. By doping with 10% *t*BuCzDBA, the hole transport ability of CBP:PPF is slightly improved and the electron transport ability of CBP:PPF is reduced, which is mainly induced by the large energy offset between CBP:PPF and *t*BuCzDBA. Meanwhile for mCBP:PPF, the dopant DMAC-DPS does not affect the hole transport ability but increases the electron transport ability. To explore the exciton allocation in all fluorescence two-color WOLEDs, we inserted an ultrathin red phosphorescent interlayer (RD071, 0.1 nm) in different positions of device W1. By observing the red emission intensity, the relative exciton density distribution is calculated (Fig. S10, ESI†). As shown in Fig. S11 (ESI†), the exciton recombination region covers the whole yellow and blue EMLs instead of being located at a narrow interface. Moreover, the exciton density distribution remains constant at different current den-

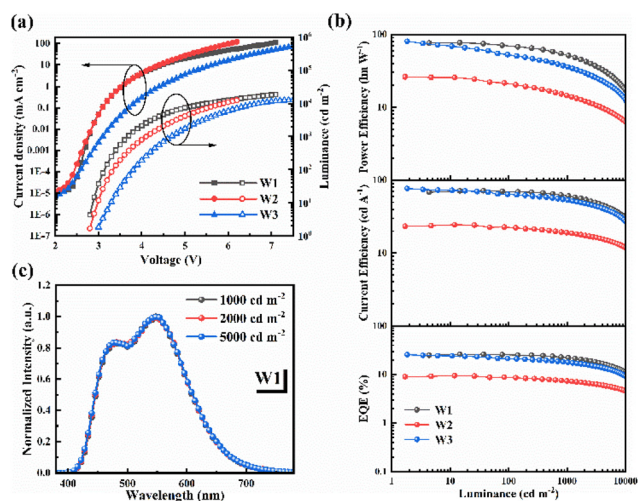


Fig. 2 (a) Current density–voltage–luminance characteristics of W1–W3. (b) CE, PE, and EQE versus luminance. (c) The normalized EL spectra of W1 at 1000, 2000, and 5000  $\text{cd m}^{-2}$ .

Table 2 EL performance of WOLEDs

Device <sup>a</sup>	$V_{\text{on}}$ <sup>b</sup> (V)	$\eta_{\text{EQE}}$ <sup>c</sup> [%]	$\eta_{\text{CE}}$ <sup>c</sup> [ $\text{cd A}^{-1}$ ]	$\eta_{\text{PE}}$ <sup>c</sup> [ $\text{lm W}^{-1}$ ]	CIE <sup>d</sup>	CRI <sup>d</sup> /max
W1	2.7	26.1/25.6/22.1	71.3/69.9/60.4	76.8/70.8/54.5	(0.31, 0.41)	64/65
W2	2.7	9.5/8.8/7.4	24.6/22.8/19.1	26.2/21.7/14.6	(0.30, 0.38)	67/68
W3	2.9	25.5/21.3/17.8	76.6/63.7/53.3	80.1/52.6/37.2	(0.33, 0.46)	59/60
W4	3.0	22.4/19.7/15.4	64.3/53.3/40.5	67.3/49.2/31.0	(0.32, 0.42)	66/67
W5	3.0	8.9/7.8/6.3	15.7/13.9/11.0	16.1/12.1/7.9	(0.29, 0.31)	83/86
W6	2.7	20.8/18.6/14.0	42.3/37.5/28.1	48.5/34.6/21.5	(0.38, 0.38)	89/91
W7	2.7	22.4/20.8/16.2	49.5/45.9/35.7	55.5/42.3/28.3	(0.37, 0.40)	90/92
W8	2.7	24.5/23.5/20.0	60.8/58.1/49.5	66.1/54.3/37.0	(0.38, 0.43)	79/80
W9	2.8	23.0/22.5/20.6	54.7/53.5/49.1	55.1/50.9/39.5	(0.35, 0.38)	89/91
W10	2.9	29.5/24.1/16.7	59.8/52.8/37.7	60.6/44.8/25.2	(0.40, 0.41)	89/90
W11	3.0	30.1/26.1/21.4	71.3/61.8/50.8	72.5/53.9/37.1	(0.42, 0.42)	84/86

<sup>a</sup> All fluorescence two-color WOLEDs of W1–W4 and all fluorescence three-color WOLEDs of W5–W11. <sup>b</sup> At a luminance of 1  $\text{cd m}^{-2}$ . <sup>c</sup> Efficiencies of the maximum, at 100  $\text{cd m}^{-2}$  and at 1000  $\text{cd m}^{-2}$ . <sup>d</sup> At a luminance of 1000  $\text{cd m}^{-2}$ .

sities. All these metrics not only suppress the exciton quenching but also provide good color stability.

Based on the above results, we conclude that the co-host system is required for both blue and yellow EMLs for complete triplet exciton harvesting and reduced exciton quenching at high luminance. Unfortunately, the limited coverage of the visible region in complementary W1 leads to a CIE of (0.31, 0.41) and a CRI of 64 at  $1000 \text{ cd m}^{-2}$  (summarized in Table 2), which is not sufficient for lighting.

### 3.3 Co-host for all fluorescence three-color WOLEDs

Following the successful application of the design strategy in all fluorescence two-color WOLEDs, all fluorescence three-color WOLEDs were developed to pursue a high CRI. A commercially available deep red fluorescent emitter with high photoluminescence quantum yield DBP is introduced to construct a sensitized TADF OLED with *t*BuCzDBA.<sup>17</sup> Similar to the two-color WOLED architecture, we inserted a red EML CBP:PPF:DBP (1:1, 0.5%, 3 nm) between the yellow and blue EMLs. With the concentration of DBP as low as 0.5%, direct carrier recombination on the fluorescent molecules of DBP by the trapping effect can be effectively suppressed despite great energy differences between co-host and DBP.<sup>38,39</sup> The all fluorescence three-color WOLED structures are ITO/HAT-CN (5 nm)/TAPC (40 nm)/TCTA (10 nm)/CBP:PPF:*t*BuCzDBA (1:1, 10%, 4 nm)/CBP:PPF:DBP (1:1, 0.5%, 3 nm)/CBP:PPF:*t*BuCzDBA (1:1, 10%, *x* nm)/mCBP:PPF:DMAC-DPS (1:1, 20%, 6 nm)/PPF (10 nm)/PBPPhen (50 nm)/Liq (2 nm)/Al (100 nm), where *x* = 0, 3, 4.5 or 6 nm are referred to W5–W8, respectively. The yellow TADF layer between blue and red EMLs is the cascaded exciton transfer layer (CETL), which plays a critical role in exciton harvesting and manipulation. The device structure and molecular structures of adopted materials are depicted in Fig. 3.

As can be seen in Fig. 4b, when there is no yellow CETL between blue and red EMLs, the device W5 reaches a maximum EQE of only 8.9%, which is much lower compared to its counterpart with yellow CETL. In device W6, a 3 nm CETL was inserted between red and blue EMLs. The EQE was dramatically improved to 20.8%, accompanied by the comparatively enhanced red emission (shown in Fig. 4c). This indicates that the yellow TADF emitter *t*BuCzDBA can not only effectively sensitize the red emitter DBP, but also suppress the triplet exciton loss from TADF emitter to fluorescent emitter DBP. By further increasing the yellow CETL to 4.5 nm and 6 nm in devices W7 and W8, respectively, the yellow emission was gradually enhanced.

As shown in Fig. 4c, when the yellow CETL was increased from 3 nm to 4.5 nm, the yellow emission increased significantly, while the red and blue emissions remained relatively unchanged. Also, the blue emission intensity can be easily tuned by changing the thickness of the blue EML. As shown in Fig. S12 (ESI<sup>†</sup>), device W9 with a blue EML thickness of 8 nm realizes increased blue emission intensity compared to W7 and keeps the yellow and red emissions relatively unchanged. These results explicitly indicate that the EL emission spectrum

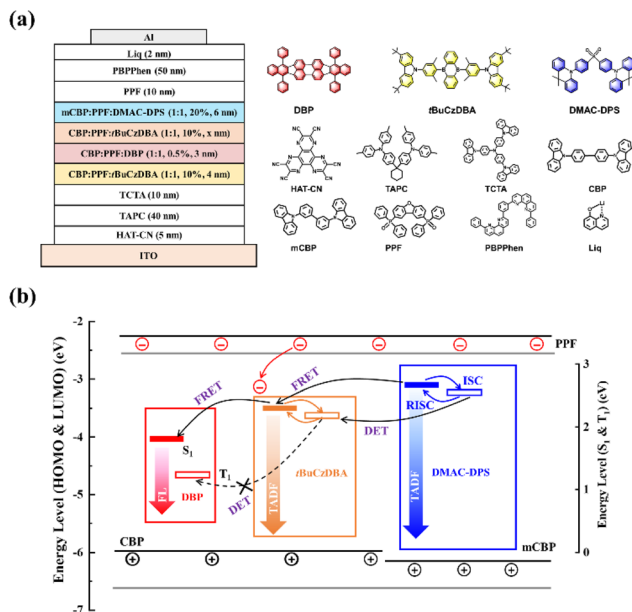


Fig. 3 (a) Device architecture and molecular structures of adopted materials. (b) The operational mechanism of three-color WOLEDs.

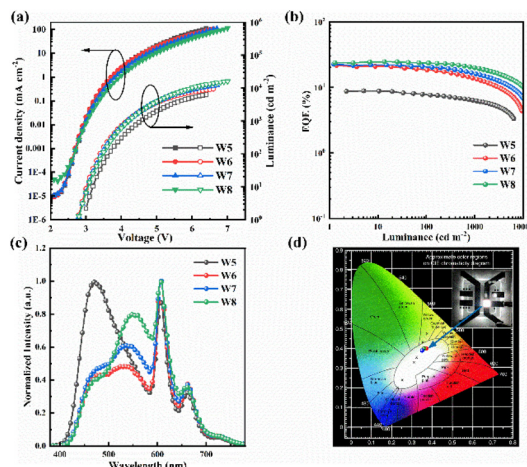


Fig. 4 (a) Current density–voltage–luminance characteristics. (b) EQE–luminance curves of all fluorescence three-color WOLEDs. (c) The normalized EL spectra of W5, W6, W7, and W8 at  $1000 \text{ cd m}^{-2}$ . (d) CIE coordinates of W7 in the luminance of 1000, 2000, and  $5000 \text{ cd m}^{-2}$ .

of the three-color WOLEDs can be independently tuned, which provides a simple but controllable strategy for optimizing the CRI. In particular, the CRI of W7 reaches 92, and the CIE coordinates are (0.37, 0.40), which is one of the highest CRIs among state-of-the-art all fluorescence WOLEDs (Table S1, ESI<sup>†</sup>). W8 shows the highest maximum EQE of 24.5%, with a qualified CRI of 80 for lighting sources. Also, the efficiency roll-off of W8 is extremely low. The EQE remains at 20.0% under  $1000 \text{ cd m}^{-2}$  (summarized in Table 2). Compared to two-color WOLEDs, three-color WOLEDs show slightly more color shifts along the luminance (Fig. 4d and Fig. S13, ESI<sup>†</sup>). For instance, W7 obtains a  $\Delta\text{CIE}$  (0.02, 0.01) when the lumi-

nance ranges from 1000 to 5000  $\text{cd m}^{-2}$ . We speculate that the red CF emitter DBP may be saturated at high luminance, which is similar to previously reported sensitized WOLEDs.<sup>40,41</sup>

The excellent device performance of three-color WOLEDs attracts us to further explore the working mechanism. To study the sensitization process, four doped films of DPEPO:20% DMAC-DPS:0.5% DBP (60 nm) (Film I), DPEPO:10% *t*BuCzDBA:0.5% DBP (60 nm) (Film II), DPEPO:20% DMAC-DPS (60 nm) (Film III), and DPEPO:10% *t*BuCzDBA (60 nm) (Film IV) were prepared. As shown in Fig. 5, the PL peaks of DMAC-DPS, *t*BuCzDBA, and DBP are located at 453, 550, and 606 nm, respectively. The transient PL decay lifetimes of DMAC-DPS (Film III) and *t*BuCzDBA (Film IV) are relatively long, exhibiting delayed fluorescence characteristics. After doping with 0.5% DBP, the transient PL decay lifetimes of DMAC-DPS in Film I and *t*BuCzDBA in Film II are significantly shortened. This can be attributed to the efficient Förster resonance energy transfer (FRET) from DMAC-DPS or *t*BuCzDBA to DBP molecules (Fig. S14, ESI<sup>†</sup>). However, as shown in Fig. S15 (ESI<sup>†</sup>), the emission/absorption overlap between *t*BuCzDBA and DBP is significantly larger than that between DMAC-DPS and DBP. This indicates the FRET rate from *t*BuCzDBA to DBP is larger than that from DMAC-DPS to DBP, resulting in higher triplet exciton density on DMAC-DPS at the same excitation value. Moreover, the symmetrically bar-shaped DMAC-DPS facilitates intermolecular interactions, leading to effect triplet diffusion from DMAC-DPS to DBP and ultimately quenching by the dark triplet state of DBP (Fig. S14, ESI<sup>†</sup>).<sup>42</sup> Combining these two synthetic effects, device W5 without yellow EML between blue and red EMLs results in serious triplet quenching and therefore low efficiency. In contrast, by inserting a CETL consisting of *t*BuCzDBA between blue TADF EML and red CF EML, the fast FRET rate from *t*BuCzDBA to DBP can effectively reduce the triplet exciton density on TADF sensitizers and subsequently suppress the Dexter energy transfer (DET) from TADF sensitizers to the CF emitter through triplet diffusion. This blocks the triplet quenching channel and endows the WOLEDs with high exciton utilization efficiency, as shown in devices W6–W8.

As mentioned above, we speculate that the red CF emitter DBP does not affect the charge transport ability of the co-host due to its low doping concentration. To confirm this hypoth-

esis, we compared the hole- and electron-only devices of the CBP:PPF with or without emitter DBP. As shown in Fig. S9a (ESI<sup>†</sup>), DBP has a negligible influence on the charge characteristics of co-host CBP:PPF. Therefore, like two-color complementary WOLEDs, the co-host system can extend the exciton generation zone to the entire EMLs, as shown in Fig. 3.

To reach sufficient red emission, red EMLs with a thickness of 3 nm are needed. The exciton recombination also takes place in the red EML. As the red EML is sandwiched by two yellow EMLs, the longest diffusion length for the triplet excitons generated in red EMLs is only 1.5 nm. As shown in Fig. S15 (ESI<sup>†</sup>), the FRET from *t*BuCzDBA to DBP is calculated to be 8.9 nm.<sup>43</sup> Therefore, all the emitters in red EMLs are in the region of the FRET radius, which ensures that all the triplet excitons generated in red EMLs are completely harvested by adjacent yellow EMLs.

To further confirm the efficient energy transfer from yellow emitter *t*BuCzDBA to red emitter DBP, we also prepared a sensitizing device YR based on the structure of ITO/HAT-CN (5 nm)/TAPC (40 nm)/TCTA (10 nm)/CBP:*t*BuCzDBA:DBP (10%:0.5%, 20 nm)/PPF (10 nm)/PBPhen (50 nm)/LiQ (2 nm)/Al (100 nm). As depicted in Fig. S16 (ESI<sup>†</sup>), the maximum EQE of device YR is 22.1% and the maximum EQE of DBP is calculated to be 18.2%. This efficiency is comparable to the best reported values for DBP,<sup>44,45</sup> indicating that triplet exciton quenching on DBP has been greatly suppressed. Therefore, the widened co-host recombination layers, efficient FRET of singlet excitons, and suppression of triplet exciton diffusion by CETL endow our proposed all fluorescence three-color WOLEDs with high efficiency and low efficiency roll-off.

### 3.4 Optical simulation for all fluorescence three-color WOLEDs

As OLEDs work in a weak microcavity, all the energy distribution channels can be quantitatively calculated. To better understand our proposed design strategy, we performed a detailed optical simulation of our optimized white OLED W7. The simulation method and detailed simulation parameters are described in Fig. S17 (ESI<sup>†</sup>). Fig. 5 shows that outcoupled EQE varies with the thicknesses of the hole transport and electron transport layers. The outcoupled EQEs for blue, yellow, and red monochrome devices are given in Fig. S18, S19, and S20 (ESI<sup>†</sup>), respectively. Fig. 6a presents the simulated spectrum of device W7 in the perpendicular direction. The photon contribution from blue, yellow, and red are 22%, 43%, and 35%, respectively. Taking a unity electron recombination rate, the maximum theoretical coupling efficiency is predicted to be 24.5%, which is quite close to our experimental value of 22.4%. This proves that our white OLEDs approach nearly 100% exciton utilization efficiency.

With a good understanding of the working mechanism of the devices, we finally prepared all fluorescence three-color WOLEDs by replacing DMAC-DPS with a highly efficient blue emitter PPCzTrz<sup>46</sup> (W10) and 5Cz-TRZ<sup>27</sup> (W11). As illustrated in Fig. 7 and Fig. S21 (ESI<sup>†</sup>), the maximum EQE of W10 and W11 reaches 29.5% and 30.1%, respectively. At 1000  $\text{cd m}^{-2}$ , the EQE remains 16.7% and 21.4%, respectively. The lower

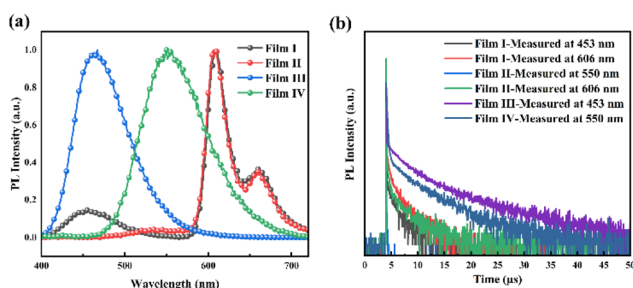


Fig. 5 (a) PL spectra of films I–IV. (b) The transient PL decay curves of films I–IV.

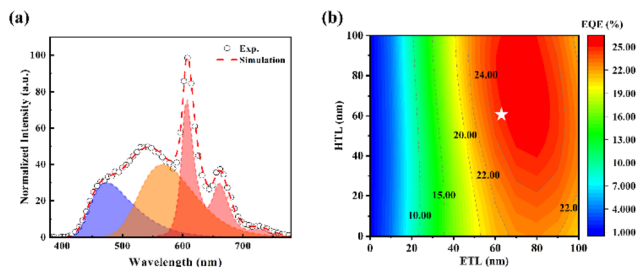


Fig. 6 (a) The experimental and theoretical EL spectra of device W7. (b) Calculated EQE as a function of the HTL and ETL thicknesses.

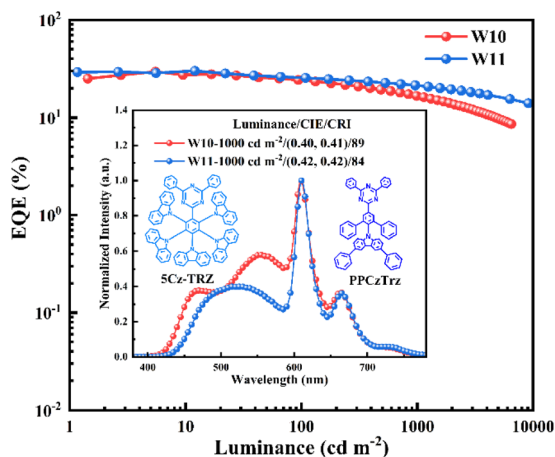


Fig. 7 EQE–luminance curve of W10 and W11. Insets: the normalized EL spectra of W10 and W11 at  $1000 \text{ cd m}^{-2}$ .

efficiency roll-off of W11 can be attributed to the fast rate of reverse intersystem crossing (RISC) of 5Cz-TRZ. Additionally, at  $1000 \text{ cd m}^{-2}$ , W10 and W11 reach CIE coordinates of (0.40, 0.41) and (0.42, 0.42), respectively, along with CRIs of 89 and 84 (shown in Table 2). These efficiencies are among the best-reported values with similar CRIs (shown in Table S1, ESI<sup>†</sup>), further validating our device design strategy.

Finally, we measured the operational stability of two-color and three-color all fluorescence WOLEDs, as shown in Fig. S22.<sup>†</sup> In the case of two-color WOLEDs, the co-host W1 exhibits a significantly 3.3 times longer  $LT_{50}$  lifetime (the time for the device degraded to 50% of the initial luminance) compared to the single-host WOLED (W4). This can be attributed to its broadened recombination zone and fuzzy interfaces, which reduce the accumulation of charges and excitons.<sup>20</sup> In the case of three-color WOLEDs, the  $LT_{50}$  value of DMAC-DPS based three-color WOLEDs at an initial luminance of  $3000 \text{ cd m}^{-2}$  reaches only 2.5 h. By replacing DMAC-DPS with a more stable material 5Cz-TRZ, the device W11 achieved an  $LT_{50}$  value of 58.6 h, which is 23 times longer than that of DMAC-DPS based white OLEDs. As unstable materials such as TAPC were adopted in the devices, the stability of our proposed device can be improved by further optimization of the materials.

## 4 Conclusions

In conclusion, we designed a monochrome yellow OLED with a maximum EQE of 31.7% by introducing a co-host system and a cascaded exciton transfer configuration in EMLs. All fluorescence two-color complementary WOLEDs based on TADF molecules reached a maximum EQE of 26.1%. With a widened exciton recombination region, two-color WOLEDs exhibit great color stability and low efficiency roll-off. More notably, by introducing red fluorescent dopant DBP and a cascaded exciton transfer layer, three-color WOLEDs achieve a maximum EQE of 22.4% and a CRI of 92. The optical simulation results prove nearly 100% exciton utilization efficiency in the proposed device architecture. With an efficient blue emitter 5Cz-TRZ, the maximum EQE of the white OLEDs is further improved to 30.1%. The excellent device performances demonstrate the feasibility of our strategy in designing highly efficient all fluorescence OLEDs with high color rendering index.

## Conflicts of interest

There are no conflicts to declare.

## Acknowledgements

We would like to thank Christian Hänisch at TU Dresden for fruitful discussions on optical simulations. This study was financially supported by the National Natural Science Foundation of China (Grant No. 62105039 and Grant No. 52103242) and the R&D Program of Beijing Municipal Education Commission (Grant No. KM202211232015). This project was also funded by the Young Elite Scientist Sponsorship Program by the China Association for Science and Technology (Grant No. YESS20200146). L. S. C. acknowledges the funding from the USTC Research Funds of the Double First-Class Initiative.

## References

- 1 C. W. Tang and S. A. VanSlyke, *Appl. Phys. Lett.*, 1987, **51**, 913.
- 2 S. Reineke, F. Lindner, G. Schwartz, N. Seidler, K. Walzer, B. Lüssem and K. Leo, *Nature*, 2009, **459**, 234.
- 3 Y. Huang, E.-L. Hsiang, M.-Y. Deng and S.-T. Wu, *Light: Sci. Appl.*, 2020, **9**, 105.
- 4 J. Zhao, Z.-H. Chi, Z. Yang, X.-J. Chen, M. S. Arnold, Y. Zhang, J.-R. Xu, Z.-G. Chi and M. P. Aldred, *Nanoscale*, 2018, **10**, 5764–5792.
- 5 M. A. Baldo, D. F. O'Brien, Y. You, A. Shoustikov, S. Sibley, M. E. Thompson and S. R. Forrest, *Nature*, 1998, **395**, 151.
- 6 Y. Liu, C. Li, Z. Ren, S. Yan and M. R. Bryce, *Nat. Rev. Mater.*, 2018, **3**, 18020.
- 7 H. Uoyama, K. Goushi, K. Shizu, H. Nomura and C. Adachi, *Nature*, 2012, **492**, 234.

- 8 Q. Wang, Y.-X. Zhang, Y. Yuan, Y. Hu, Q.-S. Tian, Z.-Q. Jiang and L.-S. Liao, *ACS Appl. Mater. Interfaces*, 2019, **11**, 2197.
- 9 Y. Fu, H. Liu, D. Yang, D. Ma, Z. Zhao and B. Z. Tang, *Adv. Opt. Mater.*, 2022, **10**, 2102339.
- 10 R. Braveenth, H. Lee, J. D. Park, K. J. Yang, S. J. Hwang, K. R. Naveen, R. Lampande and J. H. Kwon, *Adv. Funct. Mater.*, 2021, **31**, 2105805.
- 11 J. Liu, Y. Zhu, T. Tsuboi, C. Deng, W. Lou, D. Wang, T. Liu and Q. Zhang, *Nat. Commun.*, 2022, **13**, 4876.
- 12 Z. Cai, X. Wu, H. Liu, J. Guo, D. Yang, D. Ma, Z. Zhao and B. Z. Tang, *Angew. Chem.*, 2021, **133**, 23827.
- 13 Y. Liu, B. Nell, K. Ortstein, Z. Wu, Y. Karpov, T. Beryozkina, S. Lenk, A. Kiriy, K. Leo and S. Reineke, *ACS Appl. Mater. Interfaces*, 2019, **11**, 11660.
- 14 Y. Liu, C. Hänisch, Z. Wu, P.-A. Will, F. Fries, J. Wu, S. Lenk, K. Leo and S. Reineke, *J. Mater. Chem. C*, 2019, **7**, 8929.
- 15 J. Zhang, C. Han, F. Du, C. Duan, Y. Wei and H. Xu, *Adv. Funct. Mater.*, 2020, **30**, 2005165.
- 16 H. Kaji, H. Suzuki, T. Fukushima, K. Shizu, K. Suzuki, S. Kubo, T. Komino, H. Oiwa, F. Suzuki, A. Wakamiya, Y. Murata and C. Adachi, *Nat. Commun.*, 2015, **6**, 8476.
- 17 H. Nakanotani, T. Higuchi, T. Furukawa, K. Masui, K. Morimoto, M. Numata, H. Tanaka, Y. Sagara, T. Yasuda and C. Adachi, *Nat. Commun.*, 2014, **5**, 4016.
- 18 D. Zhang, L. Duan, C. Li, Y. Li, H. Li, D. Zhang and Y. Qiu, *Adv. Mater.*, 2014, **26**, 5050.
- 19 J.-H. Jou, S.-M. Shen, C.-R. Lin, Y.-S. Wang, Y.-C. Chou, S.-Z. Chen and Y.-C. Jou, *Org. Electron.*, 2011, **12**, 865.
- 20 Y. Liu, F. Liang, L.-S. Cui, X.-B. Shi, Z.-K. Wang and L.-S. Liao, *Adv. Opt. Mater.*, 2016, **4**, 2051.
- 21 T. Chatterjee and K.-T. Wong, *Adv. Opt. Mater.*, 2019, **7**, 1800565.
- 22 N. Li, F. Ni, X. Lv, Z. Huang, X. Cao and C. Yang, *Adv. Opt. Mater.*, 2022, **10**, 2101343.
- 23 A. J. Gillett, A. Pershin, R. Pandya, S. Feldmann, A. J. Sneyd, A. M. Alvertis, E. W. Evans, T. H. Thomas, L.-S. Cui, B. H. Drummond, G. D. Scholes, Y. Olivier, A. Rao, R. H. Friend and D. Beljonne, *Nat. Mater.*, 2022, **21**, 1150.
- 24 Q.-H. Zhong, S.-K. Zeng, P. Fan, Y.-D. Pang, W.-G. Zhu and Y.-F. Wang, *J. Mater. Chem. C*, 2022, **10**, 18415–18422.
- 25 D. H. Ahn, S. W. Kim, H. Lee, I. J. Ko, D. Karthik, J. Y. Lee and J. H. Kwon, *Nat. Photonics*, 2019, **13**, 540.
- 26 Y. Fu, H. Liu, D. Yang, D. Ma, Z. Zhao and B. Z. Tang, *Sci. Adv.*, 2021, **7**, eabj2504.
- 27 L.-S. Cui, A. J. Gillett, S.-F. Zhang, H. Ye, Y. Liu, X.-K. Chen, Z.-S. Lin, E. W. Evans, W. K. Myers, T. K. Ronson, H. Nakanotani, S. Reineke, J.-L. Bredas, C. Adachi and R. H. Friend, *Nat. Photonics*, 2020, **14**, 636.
- 28 C. Yin, Y. Zhang, T. Huang, Z. Liu, L. Duan and D. Zhang, *Sci. Adv.*, 2022, **8**, eabp9203.
- 29 T.-L. Wu, M.-J. Huang, C.-C. Lin, P.-Y. Huang, T.-Y. Chou, R.-W. Chen-Cheng, H.-W. Lin, R.-S. Liu and C.-H. Cheng, *Nat. Photonics*, 2018, **12**, 23.
- 30 K. Udagawa, H. Sasabe, F. Igarashi and J. Kido, *Adv. Opt. Mater.*, 2016, **4**, 86–90.
- 31 Y. Liu, L.-S. Cui, M.-F. Xu, X.-B. Shi, D.-Y. Zhou, Z.-K. Wang, Z.-Q. Jiang and L.-S. Liao, *J. Mater. Chem. C*, 2014, **2**, 2488–2495.
- 32 P. A. Vecchi, A. B. Padmaperuma, H. Qiao, L. S. Sapochak and P. E. Burrows, *Org. Lett.*, 2006, **8**, 4211–4214.
- 33 G. W. Kim, H. W. Bae, R. Lampande, I. J. Ko, J. H. Park, C. Y. Lee and J. H. Kwon, *Sci. Rep.*, 2018, **8**, 16263.
- 34 J. U. Kim, I. S. Park, C.-Y. Chan, M. Tanaka, Y. Tsuchiya, H. Nakanotani and C. Adachi, *Nat. Commun.*, 2020, **11**, 1765.
- 35 D. Chen, P. Rajamalli, F. Tenopala-Carmona, C. L. Carpenter-Warren, D. B. Cordes, C.-M. Keum, A. M. Z. Slawin, M. C. Gather and E. Zysman-Colman, *Adv. Opt. Mater.*, 2020, **8**, 1901283.
- 36 Y.-S. Park, W.-I. Jeong and J.-J. Kim, *J. Appl. Phys.*, 2011, **110**, 124519.
- 37 H. Sasabe, R. Sato, K. Suzuki, Y. Watanabe, C. Adachi, H. Kaji and J. Kido, *Adv. Opt. Mater.*, 2018, **6**, 1800376.
- 38 J. H. Lee, S. Lee, S. J. Yoo, K. H. Kim and J. J. Kim, *Adv. Funct. Mater.*, 2014, **24**, 4681.
- 39 D.-L. Zhou, G. Cheng, W.-G. Liu, S.-P. Wu and C.-M. Che, *J. Mater. Chem. C*, 2023, **11**, 3936–3943.
- 40 H. Liu, Y. Fu, B. Z. Tang and Z. Zhao, *Nat. Commun.*, 2022, **13**, 5154.
- 41 H. Liu, J. Chen, Y. Fu, Z. Zhao and B. Z. Tang, *Adv. Funct. Mater.*, 2021, **31**, 2103273.
- 42 D. Ding, Z. Wang, C. Duan, C. Han, J. Zhang, S. Chen, Y. Wei and H. Xu, *Research*, 2022, **2022**, 0009.
- 43 Y. Tang, Y. Liu, W.-M. Ning, L.-S. Zhan, J.-Q. Ding, M.-L. Yu, H.-J. Liu, Y.-H. Gao, G.-H. Xie and C.-L. Yang, *J. Mater. Chem. C*, 2022, **10**, 4637–4645.
- 44 Z. Li, X. Hu, G. Liu, L. Tian, H. Gao, X. Dong, T. Gao, M. Cao, C.-S. Lee and P. Wang, *J. Phys. Chem. C*, 2021, **125**, 1980.
- 45 K. Rayappa Naveen, C. P. K. Prabhu, R. Braveenth and J. Hyuk Kwon, *Chem. – Eur. J.*, 2022, **28**, e202103532.
- 46 S. O. Jeon, K. H. Lee, J. S. Kim, S.-G. Ihn, Y. S. Chung, J. W. Kim, H. Lee, S. Kim, H. Choi and J. Y. Lee, *Nat. Photonics*, 2021, **15**, 208–215.